 Printed in China Communications in Theoretical Physics

Commun. Theor. Phys. **77** (2025) 075407 (13pp) https://doi.org/10.1088/1572-9494/ada87d
CSTR: 32041.14.CTP.ada87d

Rotating regular black holes in AdS spacetime and its shadow for an arbitrary observer

Balendra Pratap Singh[1,2,*], **Md Sabir Ali**[3,4] **and Sushant G Ghosh**[5,6]

[1] Department of Physics, Applied Science Cluster, SOAE, UPES, Energy Acres, Bidholi, Via Prem Nagar, Dehradun, Uttarakhand, 248007, India
[2] Department of Applied Sciences and Engineering, Tula's Institute, Dehradun, Uttarakhand 248197, India
[3] Department of Physics, Mahishadal Raj College, West Bengal 721628, India
[4] Indian Institute of Science Education and Research Kolkata, West Bengal 741246, India
[5] Centre for Theoretical Physics, Jamia Millia Islamia, New Delhi 110025, India
[6] Astrophysics and Cosmology Research Unit, School of Mathematics, Statistics and Computer Science, University of KwaZulu-Natal, Private Bag 54001, Durban 4000, South Africa

E-mail: balendrap.singh@ddn.upes.ac.in, alimd.sabir3@gmail.com, sghosh2@jmi.ac.in and sgghosh@gmail.com

Received 24 June 2024, revised 13 December 2024
Accepted for publication 10 January 2025
Published 7 April 2025

Abstract

The photon region surrounding a black hole is crucial for distant observers to receive the emitted spectrum from its vicinity. This paper investigates the optical features of a regular spinning anti-de Sitter (AdS) black hole. These kinds of black holes hold deviation parameter k, and the cosmological constant Λ including their mass M and spin a. The cosmological parameter depends on the curvature radius by $\Lambda = -3/l^2$. We investigate the structure of geodesics for unstable circular orbits of photons as observed by an observer at specific Boyer-Lindquist coordinates $(r_O,\ \vartheta_O)$ in the region between the outer and cosmological horizon, so-called the domain of outer communication. Our investigations include the analysis of three observables from its shadow plot: the black hole shadow radius (R_s), the distortion of the black hole (δ_s), and shadow area A. With the help of these observables, we calculate the angular diameter of the apparent size of the shadow. The shadows cast by spinning regular spacetimes are smaller compared to those produced by rotating black holes in both general relativity and regular spacetimes. We also calculate the rate at which energy is emitted from the black hole.

Keywords: regular black hole, black hole shadow, null geodesics and photon orbits

(Some figures may appear in colour only in the online journal)

1. Introduction

Observing the shadow of a black hole provides a significant opportunity to study its characteristics and parameters. The paths of light particles around a black hole are impacted by their angular momentum. Photons with higher angular momentum scatter away from the black hole and can reach a distant observer at infinity. In contrast, photons with lower angular momentum are drawn into the black hole, resulting in a dark area that defines the shadow region around the horizons of the black hole. The black hole shadow forms near the event horizon, providing insight into the basic geometrical structure of horizons. Recent astronomical observations from the Event Horizon Telescope (EHT) confirm the existence of the black hole Sagittarius A* in our galaxy Milky Way [1–6] and a supermassive black hole at the galactic center of Messier 87 [7–12]. The shadow of a black hole appears as a two-dimensional dark region surrounded by electromagnetic radiation and matter particles. The dark region occurs due to the infalling photons inside the event horizon while the photons that form orbits can be visible to an outside observer. The shadow figure depends on black hole parameters as well as the surrounding matter field around the black hole. Therefore, the

* Author to whom any correspondence should be addressed.

study of the shadow figure is a valuable tool for detecting its spin and other deformation parameters, as its shape and size reflect the geometry surrounding the black hole. Astrophysical black hole candidates exhibit a significant amount of rotation. This drives our interest in studying rotating black holes and their shadows. Since regular black holes include the Kerr metric as a special case, we view them as prototypes for a broader category of non-Kerr families. In these cases, the metric retains the same form, but the mass parameter M is replaced with a function $m(r)$. This method is very useful for studying the various parameters associated with black holes in the general theory of relativity, as well as in different theories of gravity. It also provides an opportunity to test these theories using astrophysical black holes. In general relativity, the shape and size of a black hole's shadow are determined solely by its spin and mass [13, 14]. However, in alternative theories of gravity, the shadow of a black hole can be influenced by various other parameters. Therefore, it is worthwhile to investigate the properties of black hole shadows within different modified gravitational theories. Over the past few years, various researchers have explored this topic in modified theories of gravity such as [15–52]. The properties of black hole shadows are affected by nearby matter fields, which has led to investigations into these shadow characteristics in plasma conducted by [53–55]. The intriguing aspect of a black hole's shadow has been investigated in higher-dimensional spacetime [56–60]. Cunha *et al* [61, 62] developed a ray tracing method to better understand photon rays in the vicinity of Kerr spacetime, both with and without scalar hair.

In this article, we consider an observer positioned in an arbitrary location rather than at infinity, and we trace various shadow images cast by regular anti-de Sitter (AdS) black holes as seen by that observer. The articles [34, 63] examine the shadow images cast by Kerr-Newman-NUT-AdS black holes and rotating AdS black holes within the braneworld scenario. Additionally, [64, 65] investigated the shadows of superentropic and Bardeen black holes in AdS spacetime. The current cosmological observations verified that our Universe is accelerating and considering that accelerating, [66, 67] investigated the shadows of rotating black with the cosmological constant. In this article, we present a detailed analysis of the shadows of rotating regular AdS black holes. Our focus is primarily on how the spin and deformation parameters affect the characteristics of the black hole shadow. Compared to the shadows produced by Kerr [13] and nonsingular [21] black holes, the shadow of a rotating regular AdS black hole is smaller and appears more distorted.

This paper is organized as follows: section 2 describes the properties of the rotating regular AdS black hole. In section 3, we calculate the equations of motion for the geodesics of photons. Following that, in section 4, we present various shadow images. Additionally, we estimate the energy emission rate and conclude with our final remarks in section 6.

2. A brief overview of the rotating regular AdS black hole

This section focuses on the spacetime structure of regular black holes that are minimally coupled to a nonlinear source term in the presence of a negative cosmological constant. We will start by discussing the static spacetime metric, which possesses spherical symmetry. Following this, we will review the rotating counterparts of these solutions in Anti-de Sitter (AdS) spacetime. We will describe a four-dimensional static black hole that maintains spherical symmetry as defined by

$$\mathrm{d}s^2 = -f(r)\mathrm{d}t^2 + \frac{\mathrm{d}r^2}{f(r)} + r^2\mathrm{d}\Omega_2^2, \tag{1}$$

where function $f(r)$ is the radial dependent metric function and the line element on a two-dimensional sphere with unit radius is given by $\mathrm{d}\Omega_2^2 = \mathrm{d}\theta^2 + \sin^2\theta\mathrm{d}\phi^2$. The action that describes the regular AdS black hole solution of our interest is best formulated as follows, as defined in the works by [68, 69]

$$\mathcal{I} = \int \mathrm{d}^4x\sqrt{-g}\,[R - \mathcal{L}(\mathcal{F}) + 6l^{-2}]. \tag{2}$$

The action of the black hole, as mentioned in the equation above, has a Ricci scalar quantity R and a radius of curvature l that is related to the cosmological constant by $\Lambda = -3/l^2$ and $\mathcal{L}(\mathcal{F})$ is the Lagrangian that includes a nonlinear electromagnetic source and can be described as [68, 69]

$$\mathcal{L}(\mathcal{F}) = \mathrm{e}^{[-s(2g^2\mathcal{F})^{\frac{1}{4}}]}\mathcal{F}, \tag{3}$$

with $\mathcal{F} = F_{\mu\nu}F^{\mu\nu}/4$, and $F_{\mu\nu} = 2\nabla_{[\mu}A_{\nu]}$. We choose for the sake of clarity, $s = q/2M$, where q and M are the electric charge and mass of the black hole respectively [70, 71]. The following equations can be obtained by the verification of black hole action $\mathcal{I}$ concerning the metric tensor $g_{\mu\nu}$ and vector potential A_μ as

$$\begin{aligned} G_{\mu\nu} - \tfrac{3}{l^2} &= T_{\mu\nu}, \\ \nabla_\mu\left(\tfrac{d\mathcal{L}(\mathcal{F})}{d\mathcal{F}}F^{\nu\mu}\right) &= 0, \\ \nabla_\mu(^*F^{\mu\nu}) &= 0, \end{aligned} \tag{4}$$

where the stress-energy tensor, $T_{\mu\nu}$ for the nonlinear source concerned is given as

$$T_{\mu\nu} = 2\left[\frac{d\mathcal{L}(\mathcal{F})}{d\mathcal{F}}F_{\mu\alpha}F^{\alpha}_{\nu} - g_{\mu\nu}\mathcal{L}(\mathcal{F})\right]. \tag{5}$$

The form of the Faraday tensor $F_{\mu\nu}$ is written as the following *ansatz* [70]

$$F_{\mu\nu} = 2\delta^{\theta}_{[\mu}\delta^{\phi}_{\nu]}q(r)\sin\theta. \tag{6}$$

The dual electromagnetic field equation, $\nabla_\mu(^*F^{\mu\nu}) = 0$ alternatively follows $\mathrm{d}F = 0$, and that follows $q'(r)\mathrm{d}r \wedge \mathrm{d}\theta \wedge \mathrm{d}\phi = 0$, and leads to $q(r) = \text{constant} = q$ [70]. The resulting Maxwell tensor can have only one component [70],

$$F_{\theta\phi} = -q\sin\theta, \tag{7}$$

and

$$\mathcal{F} = \frac{q^2}{2r^4}. \tag{8}$$

Therefore, the Lagrangian (3) reads [69, 72],

$$\mathcal{L}(\mathcal{F}) = \frac{q^2}{2r^4}\mathrm{e}^{-\frac{q^2}{2Mr}}. \tag{9}$$

When we solved the zeroth component of the Einstein field

equations (4) with the energy-momentum tensor (5) and the Lagrangian (9), we get the metric function with $q^2 = 2Mk$, having the form [68, 69, 72]

$$f(r) = 1 - \frac{2M\ \mathrm{e}^{-\frac{k}{r}}}{r} + \frac{r^2}{l^2}. \tag{10}$$

Through the following calculations, we obtained the regular black hole metric in AdS spacetime, which is given by [68, 69]

$$\begin{aligned} \mathrm{d}s^2 = &-\left(1 - \frac{2M\ \mathrm{e}^{-\frac{k}{r}}}{r} + \frac{r^2}{l^2}\right)\mathrm{d}t^2 \\ &+ \frac{1}{\left(1 - \frac{2M\ \mathrm{e}^{-\frac{k}{r}}}{r} + \frac{r^2}{l^2}\right)}\mathrm{d}r^2 + r^2\mathrm{d}\Omega_2^2. \end{aligned} \tag{11}$$

Next, we derive the rotating solution for the regular AdS spacetimes, as described in equation (11). The equation of gauge potential for a nonlinear rotating charged black hole is given by [73, 74]

$$A_\mu = -\frac{g\ a\ \cos\theta}{\Upsilon}\delta^t_\mu + \frac{g(r^2 + a^2)\cos\theta}{\Upsilon}\delta^\phi_\mu. \tag{12}$$

In the absence of the spin parameter, the expression of the gauge potential reduces for the spherically symmetric spacetime as follows $A_\mu = g\cos\theta\delta^\phi_\mu$. The gauge potential (12) in the rotational case, have Maxwell field invariant [73]

$$\mathcal{F} = \frac{2g^2((\Upsilon - 2r^2)^2 - 4a^2r^2\cos^2\theta)}{\Upsilon^4}. \tag{13}$$

We derive the expressions for the Lagrangian and its derivative with respect to the Maxwell field invariant [73] by solving any two independent components of the Einstein field equations given by

$$\begin{aligned} \mathcal{L}(r) &= \frac{4r^2(2r^2\Upsilon\, m'' + 5\, m'((\Upsilon - 2r^2)^2 - 8r^2\Upsilon + 4r^2))}{\Upsilon^4}, \\ \frac{\mathrm{d}\mathcal{L}(r)}{\mathrm{d}\mathcal{F}} &= \frac{r\Upsilon\, m'' + 2m'(\Upsilon - 2r^2)}{2g^2}, \end{aligned} \tag{14}$$

with the $'$ and $''$ denoting, are the first and second derivative with respect to the radial coordinate r. The regular rotating black holes are defined by their mass, spin, and nonlinear parameters. We consider the rotating regular black hole in Boyer-Lindquist coordinates. In these coordinates, the black hole takes the form of the Kerr metric with additional parameters.

Subsequent discussion is devoted to the stationary axisymmetric regular AdS black hole solutions. The rotating regular black hole metric in AdS spacetime, expressed in Boyer-Lindquist coordinates, is best described by

$$\begin{aligned} \mathrm{d}s^2 = &-\frac{\in_r}{\Upsilon}\left(\mathrm{d}t - \frac{a\sin^2\theta}{\Xi}\mathrm{d}\phi\right)^2 + \frac{\Upsilon}{\in_r}\mathrm{d}r^2 + \frac{\Upsilon}{\in_\theta}\mathrm{d}\theta^2 \\ &+ \frac{\in_\theta \sin^2\theta}{\Upsilon}\left(a\mathrm{d}t - \frac{a^2 + r^2}{\Xi}\mathrm{d}\phi\right)^2, \end{aligned} \tag{15}$$

with

$$\Upsilon = r^2 + a^2\cos^2\theta, \quad \in_r = (r^2 + a^2)\left(1 + \frac{r^2}{l^2}\right) - 2Mr\mathrm{e}^{-k/r}, \tag{16}$$

and

$$\in_\theta = 1 - \frac{a^2}{l^2}\cos^2\theta, \quad \Xi = 1 - \frac{a^2}{l^2}. \tag{17}$$

The above black hole metric (15) is parameterized by four distinct parameters that are its mass M, spin a, the free parameter k, and the curvature radius l, and in the absence of cosmological constant the black metric reduces to the rotating nonsingular spacetime [75]. The rotating black hole metric (15) simplifies to the Kerr-AdS black hole when $k = 0$, and further simplifies to the Kerr black hole when $\Lambda = 0$. The black hole spacetime metric (15) shows singularity at $\Upsilon = 0$ and $\in_r = 0$, but $\in_r = 0$ is coordinate-dependent singularity and can be easily removable by taking a proper coordinate transformation. For $k \ll r$ the black hole metric (15) is reduced for the Kerr-Newman-AdS black hole metric such that [76]

$$\in_r = (r^2 + a^2)\left(1 + \frac{r^2}{l^2}\right) - 2Mr + q^2 + \mathcal{O}(k^2/r^2). \tag{18}$$

The determinant of the metric (15) has the form

$$\sqrt{-g} = \frac{\Upsilon\sin\theta}{\Xi}. \tag{19}$$

Since the spacetime metric equation (15) has no time t and azimuthal coordinates ϕ, hence it corresponds two communicating Killing vectors, $\xi^\mu(t) = \delta^\mu t$, and $\xi^\mu_{(\phi)} = \delta^\mu_\phi$ and that satisfies the Killing equation, $\xi_{\mu;\nu} + \xi_{\nu;\mu} = 0$. The various metric components are evaluated as a scalar product of these Killing vectors such that

$$\xi^\mu_{(t)}\,\xi_{(t)_\mu} = g_{tt} = -1 + \frac{2Mr\mathrm{e}^{-k/r}}{\Upsilon} - \frac{r^2 + a^2\sin^2\theta}{l^2}, \tag{20}$$

$$\xi^\mu_{(t)}\,\xi_{(\phi)_\mu} = g_{t\phi} = -\frac{a\sin^2\theta}{\Xi}\left(\frac{2Mr\mathrm{e}^{-k/r}}{\Upsilon} - \frac{r^2 + a^2}{l^2}\right), \tag{21}$$

$$\xi^\mu_{(\phi)}\,\xi_{(\phi)_\mu} = g_{\phi\phi} = \frac{\sin^2\theta}{\Xi}\left((r^2 + a^2)\Xi + \frac{2Mra^2\sin^2\theta\mathrm{e}^{-k/r}}{\Upsilon}\right). \tag{22}$$

Now, let us consider the Einstein field equations

$$G_{\mu\nu} = R_{\mu\nu} - \frac{1}{2}Rg_{\mu\nu} + \Lambda g_{\mu\nu} = 8\pi T_{\mu\nu}, \tag{23}$$

and by examining the above field equations, we have the Einstein tensor as [77]

$$
\begin{aligned}
G_{tt} &= \frac{2[r^4m' - 2r^3m'm + a^2r^2m' - a^4\sin^2\theta m'\cos^2\theta]}{\Upsilon^3} \\
&\quad - \frac{ra^2\sin^2\theta m''}{\Upsilon^2} + \Lambda\frac{a^2\sin^2\theta - \in_r}{\Upsilon}, \\
G_{rr} &= -\frac{2r^2m'}{\Upsilon\in_r} + \Lambda\frac{\Upsilon}{\in_r}, \\
G_{\theta\theta} &= -\frac{2a^2\cos^2\theta m'}{\Upsilon} - rm'' + \Lambda\Upsilon, \\
G_{t\phi} &= \frac{2a\sin^2\theta[(r^2+a^2)m'(a^2\cos^2\theta - r^2)]}{\Upsilon^3} \\
&\quad - \frac{ra^2\sin^2\theta(r^2+a^2)m''}{\Upsilon^2} + \Lambda\frac{a\sin^2\theta[\in_r - r^2 - a^2]}{\Upsilon}, \\
G_{\phi\phi} &= -\frac{\sin^2\theta[(r^2+a^2)a^2(a^2+(2r^2+a^2)\cos 2\theta) + r^3 2\sin^2\theta m)]}{\Upsilon^3} \\
&\quad - \frac{r\sin^2\theta m''(r^2+a^2)^2}{\Upsilon^2} \\
&\quad + \Lambda\frac{\sin^2\theta[(r^2+a^2)^2 - a^2\in_r]}{\Upsilon}.
\end{aligned}
\tag{24}
$$

The black hole spacetime has Killing vector fields $\xi^{\mu}_{(t)}$ and $\xi^{\mu}_{(\phi)}$, which arise from the symmetries of the spacetime. These Killing vectors represent null generators of the event horizon and are also tangent to the null surfaces of the event horizon. The angular velocity Ω_+ at the event horizon of a black hole is expressed in the following form

$$\Omega_+ = \frac{a\Xi}{a^2 + R_+^2}. \tag{25}$$

The angular velocity of the observer moving on the fixed orbits with constant radius can be derived using the four-velocity u^{μ} such that $u^{\mu}\xi_{(\phi)_{\mu}} = 0$ and that gives

$$\Omega = -\frac{g_{t\phi}}{g_{\phi\phi}} = \frac{a\Xi((r^2+a^2)\in_\theta - \in_r)}{(r^2+a^2)^2\in_\theta - a^2\sin^2\theta\in_r}. \tag{26}$$

As the horizon radius approaches the black hole's outer horizon, the equation for angular velocity (26) simplifies to equation (25). In the asymptotic limit, the equation of the angular velocity does not vanish and yields a finite value as follows

$$\Omega_\infty = -\frac{a}{l^2}. \tag{27}$$

By using equations (26) and (27), we derive a more relevant expression for the angular velocity of the black hole in the frame that is static at asymptotic infinity.

$$\omega_+ = \Omega_+ - \Omega_\infty = \frac{a}{a^2 + R_+^2}\left(1 + \frac{R_+^2}{l^2}\right). \tag{28}$$

The angular velocity discussed in equation (28) is one of the most important characteristics of rotating AdS black holes. It plays a crucial role in deriving a consistent first law of black hole thermodynamics, particularly in relation to the Smarr relation. It can also be demonstrated that the angular velocity, as described in equation (28), aligns with the angular velocity of the boundary Einstein universe. This provides a relevant basis within the context of the AdS/CFT duality concerning any rotating AdS black hole.

The metric (15) belongs to the prototype of a non-Kerr black hole encompassing the Kerr black holes as a special case ($k = 1/l^2 = 0$). The regular rotating black holes modeled as the non-Kerr black holes put some bounds on the spin parameter and the deviation parameter k to behave like a Kerr black hole mimickers. Consequently, the spacetime geometry around the black hole candidates modeled as the Kerr black holes using the radio and x-ray data [78–81] shows us a possible deviation from the black hole in general relativity. Proceeding along this line we consider the regular rotating AdS black hole candidates which may discard or constrain possible deviations from the Kerr background.

3. Null geodesics

In this section, we derive the null geodesics around regular AdS spacetime. For this purpose, we consider the Hamilton–Jacobi equation given by [82]:

$$\frac{\partial\mathcal{S}}{\partial\sigma} = -\frac{1}{2}g^{\alpha\beta}\frac{\partial\mathcal{S}}{\partial x^\alpha}\frac{\partial\mathcal{S}}{\partial x^\beta}. \tag{29}$$

Here in the above Hamilton–Jacobi equation Υ is the affine parameter. The black hole metric has two conserved quantities from the symmetries of spacetime, which have the dimensions of energy (E) and angular momentum (L), respectively. To derive all the equations of motion, we select a separable solution defined as [83]

$$\mathcal{S} = \frac{1}{2}m_0{}^2\sigma - Et + L\phi + \mathcal{S}_r(r) + \mathcal{S}_\theta(\theta). \tag{30}$$

Where in the above separable solution m_0 is the mass of the test particle and null geodesics its value is zero. By using the separable solution (30) in the Hamilton–Jacobi equation (29) we obtain the complete geodesics equations for the electromagnetic radiations around the black hole as

$$
\begin{aligned}
\Upsilon\frac{\mathrm{d}t}{\mathrm{d}\sigma} &= \frac{r^2+a^2}{\in_r}[E(r^2+a^2) - a\Xi L] \\
&\quad - \frac{a}{\in_\theta}(aE\sin^2\theta - \Xi L),
\end{aligned}
\tag{31}
$$

$$\Upsilon\frac{\mathrm{d}\phi}{\mathrm{d}\sigma} = \frac{a\Xi}{\in_r}[E(r^2+a^2) - a\Xi L] - \frac{\Xi}{\in_\theta}(aE - \Xi L\csc^2\theta), \tag{32}$$

$$\Upsilon^2\frac{\mathrm{d}^2r}{\mathrm{d}\sigma^2} = R_r, \tag{33}$$

and

$$\Upsilon^2\frac{\mathrm{d}^2\theta}{\mathrm{d}\sigma^2} = \Theta_\theta, \tag{34}$$

in the above geodesics equations (33) and (34), the expressions of R and Θ are defined as

$$R_r = [(a^2+r^2)E - a\Xi L]^2 - [(L - aE)^2 + \mathcal{K}]\in_r, \tag{35}$$

$$\Theta_\theta = -(a\sin^2\theta - \xi\Xi)^2\csc^2\theta - [(\xi - a)^2 + \mathcal{K}]\in_\theta. \tag{36}$$

For the separation of radial and angular geodesics equations, we use a separating constant $\mathcal{K}$ that is also called the Carter

separable constant. The Carter separable constant has the dimensions of the angular momentum. The above geodesic equations describe the motion of all frequencies of electromagnetic radiation around the rotating AdS black hole spacetimes. Now we are interested in analyzing these radiations and for that, it's required to define two impact parameters: $\xi = L/E$ and $\eta = \mathcal{K}/E^2$. After substituting these impact parameters in equation (33), the equation takes the following form

$$R_r = [(a^2 + r^2) - a\xi\Xi]^2 - [(\xi - a)^2 + \eta] \in_r . \tag{37}$$

To obtain the innermost unstable orbits we maximize the radial equation of motion equation (33)

$$\mathcal{R}(r) = \frac{\mathrm{d}R_r}{\mathrm{d}r} = 0, \tag{38}$$

we can separate the impact parameters by solving the above equation (38) simultaneously and that follows

$$\xi(r_{ph}) = \frac{-4r_{ph} \in_r + (r_{ph}^2 + a^2) \in_r{}'}{a\Xi \in_r{}'}, \tag{39}$$

$$\eta(r_{ph}) = \frac{-16r_{ph}^2 \in_r^2 - \left(r_{ph}^2 + \frac{a^4}{l^2}\right)^2 \in_r{}'^2 + 8r_{ph} \in_r \left(2a^2 r_{ph}\Xi^2 + \left(r_{ph}^2 + \frac{a^4}{l^2}\right) \in_r{}'\right)}{a^2\Xi^2 \in_r{}'^2}, \tag{40}$$

where the term $\in_r{}'$ denotes the derivative of $\in_r$ with respect to r at point $r = r_{ph}$ and it can be written as

$$\in_r{}' = -\frac{2}{3}\Big(3(M\mathrm{e}^{-k/r_{ph}}(k + r_{ph})/r_{ph}) - 3r_{ph} - \frac{1}{3l^2}r_{ph}(a^2 + 2r_{ph}^2)\Big). \tag{41}$$

The geometry of electromagnetic radiations of all frequencies around regular AdS black holes can be traced by the impact parameters given in equations (39) and (40). In the limit of $\Lambda = 0$, these impact parameters reduce to the expressions for nonsingular spacetime [21] as

$$\xi = \frac{3M(a^2(k + r_{ph}) + r_{ph}^2(k - 3r_{ph})) + 3r_{ph}^2(a^2 + r_{ph}^2)\mathrm{e}^{k/r_{ph}}}{3aM(k + r_{ph}) - 3ar_{ph}^2\mathrm{e}^{k/r_{ph}}}, \tag{42}$$

$$\eta = -\frac{r_{ph}^4(4a^2M\mathrm{e}^{k/r_{ph}}(k - r_{ph}) + (r_{ph}(r_{ph}\mathrm{e}^{k/r_{ph}} - 3M) + kM)^2)}{a^2(r_{ph}(M - r_{ph}\mathrm{e}^{k/r_{ph}}) + kM)^2}, \tag{43}$$

and which in addition, for $k = 0$ exactly reduces to the Kerr spacetime such that

$$\xi = \frac{a^2(M + r_{ph}) + r_{ph}^2(r_{ph} - 3M)}{a(M - r_{ph})}, \tag{44}$$

$$\eta = -\frac{r_{ph}^3(r_{ph}(r_{ph} - 3M)^2 - 4a^2M)}{a^2(M - r_{ph})^2}. \tag{45}$$

One can analytically study the photon orbits by using the equations (39) and (40) around regular black holes in AdS spacetimes. To obtain the figures of black hole shadow observed at some finite distance by an arbitrary observer, one has to use the coordinates, say $(r_O,\ \vartheta_O)$, and these coordinates are related to the orthonormal tetrads.

4. Rotating regular AdS black hole shadow

In this section, we figure out the images of the black hole shadow and perform related analysis. We fix the observer position somewhere between the outer and cosmological horizons in Boyer–Lindquist coordinates $(r_O,\ \vartheta_O)$. We define the orthonormal tetrads at $(r_O,\ \vartheta_O)$ as [34, 63, 84, 85]

$$e_0 = \frac{(r^2 + a^2)\partial_t + a\Xi\partial_\phi}{\sqrt{\in_r \Upsilon}}\Bigg|_{(r_O,\vartheta_O)}, \quad e_1 = \sqrt{\frac{\in_\theta}{\Upsilon}}\,\partial_\theta\Bigg|_{(r_O,\vartheta_O)}, \tag{46}$$

and

$$e_2 = -\frac{\Xi\partial_\phi + a\sin^2\theta\partial_t}{\sqrt{\in_\theta \Upsilon}\sin\theta}\Bigg|_{(r_O,\vartheta_O)}, \quad e_3 = -\sqrt{\frac{\in_r}{\Upsilon}}\,\partial_r\Bigg|_{(r_O,\vartheta_O)}, \tag{47}$$

where e_0 and e_3 denote the four velocities of the observer which gives the spatial direction towards the black hole and the combination $e_0 \pm e_3$ is tangential to the outgoing and ingoing principal null congruences of the metric. The coordinates $\S(s) = (r(s), \theta(s), \phi(s), t(s))$ be assigned for each light ray which in turn gives its tangent vector as

$$\dot{\S} = \dot{r}\partial_r + \dot{\theta}\partial_\theta + \dot{\phi}\partial_\phi + \dot{t}\partial_t, \tag{48}$$

and the tangent vector is

$$\dot{\S} = p(-e_0 + \cos\beta\sin\alpha e_1 + \sin\beta\sin\alpha e_2 + \cos\alpha e_3). \tag{49}$$

From equations (48) and (49), the scale factor p can be calculated as

$$\S = n(\dot{\S}, e_0) = n\left(\dot{\lambda}, \frac{r^2 + a^2}{\sqrt{\in_r \Upsilon}}\partial_t + \frac{a\Xi}{\sqrt{\in_r \Upsilon}}\partial_\phi\right) = \frac{-E(r^2 + a^2) + a\Xi L}{\sqrt{\in_r \Upsilon}}\Bigg|_{(r_O,\vartheta_O)}, \tag{50}$$

and by comparing the corresponding coefficients in equations (48) and (49), we have

$$\alpha = \arcsin\left(\frac{\sqrt{[(\xi(r_{ph}) - a)^2 + \eta(r_{ph})]\in_r}}{r^2 + a^2 - a\Xi\xi(r_{ph})}\Bigg|_{(r_O,\vartheta_O)}\right), \tag{51}$$

and

$$\beta = \arcsin\left(\frac{\sqrt{\in_r}\sin\theta}{\sqrt{\in_\theta}\sin\alpha}\left[\frac{a - \Xi\xi(r_{ph})\csc^2\theta}{a\Xi\xi(r_{ph}) - (r^2 + a^2)}\right]\Bigg|_{(r_O,\vartheta_O)}\right). \tag{52}$$

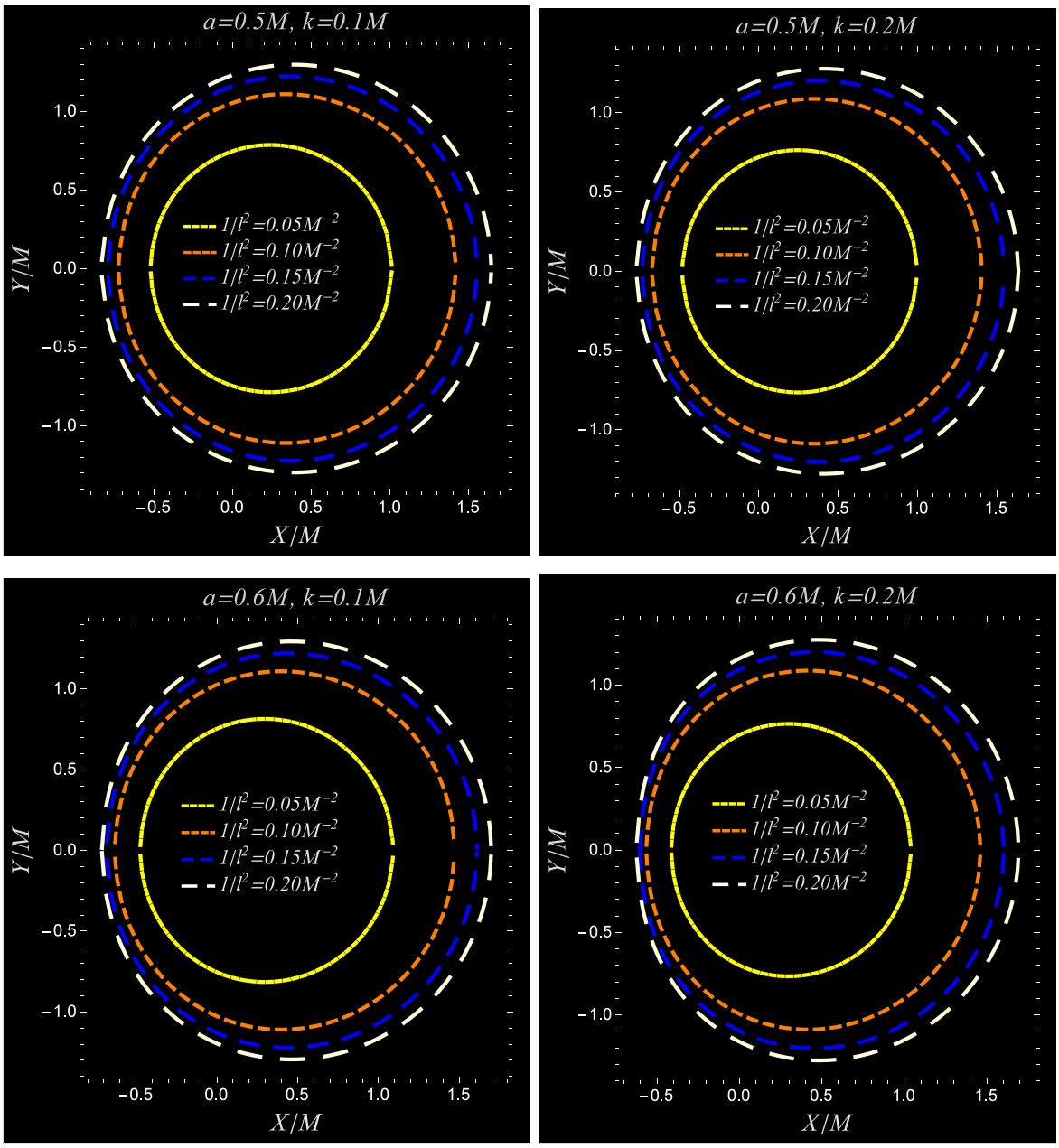

Figure 1. Plot showing the black hole shadow in rotating regular AdS spacetime at $r_O = 50$ and for different values of k, a and $1/l^2$.

In order to obtain the apparent shape of the shadow, we have considered the stereographic projection of the celestial sphere onto a plane, as shown in figure 4, where the Cartesian coordinates in this plane take the form

$$X = -2\tan\left(\frac{\alpha(r_{ph})}{2}\right)\sin\left(\beta(r_{ph})\right),$$
$$Y = -2\tan\left(\frac{\alpha(r_{ph})}{2}\right)\cos\left(\beta(r_{ph})\right), \tag{53}$$

which satisfies the relation

$$X^2 + Y^2 = 4\tan^2\left(\frac{\alpha(r_{ph})}{2}\right). \tag{54}$$

One can obtain the figure of the black hole shadow by simply taking the contour of equation (54). The figure of the black hole shadow depends primarily on its spin parameter a, curvature radius $1/l^2$, and the free parameter k. We show the figures of black hole shadow in figures 1, 2, and 3 for different values of a, $1/l^2$, and k. The figure of the black hole shadow emphasizes that the size and distortion of the shadow images increases with the $1/l^2$ (cf figure 1) while its size decreases with k (cf figure 2). We also plot the spherical ($a = 0$) regular AdS black hole shadow in figure 3 which appears as a perfect circle and increases with the increasing values $1/l^2$.

For the analysis of the shadow figures we define observable: one is the shadow radius R_s and another is the

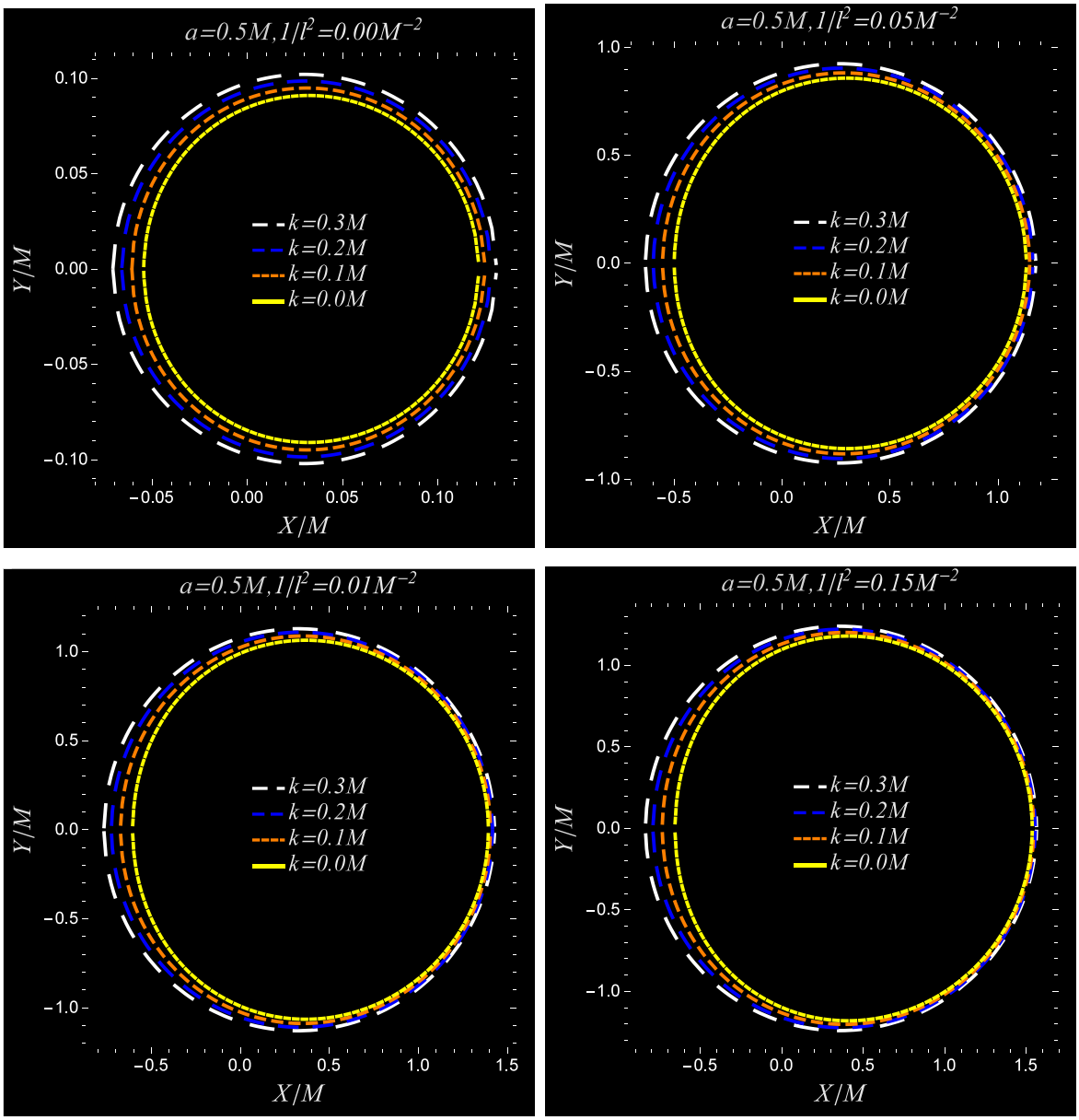

Figure 2. Plot showing the black hole shadow in rotating regular AdS spacetime at $r_O = 50$ and for different values of k, a, and $1/l^2$.

distortion parameter of the shadow figure δ_s given by [23]

$$R_s = \frac{(X_t - X_r)^2 + Y_t^2}{2|X_t - X_r|}, \tag{55}$$

where $(X_t,\ Y_t)$ and $(X_r,\ Y_r)$ are the topmost and the rightmost positions of the celestial coordinates from where the contour passes from the axes. The second observable δ_s reads

$$\delta_s = \frac{D_s}{R_s}. \tag{56}$$

The variation of the shadow radius and the distortion parameter is shown in figure 5. The shadow radius and distortion parameter increase monotonically with the radius of curvature parameter $1/l^2$ for fixed a (cf. figure 5). In figure 6 we plot the shadow radius R_s and distortion parameter δ_s in $(a,\ 1/l^2)$ plane. The point of intersection of R_s and δ_s lines gives the spin parameter a and radius of curvature parameter $1/l^2$. If we compare our results with those of nonsingular black hole shadows [21], we find that in AdS spacetime, the size of the black hole shadow appears larger and becomes more distorted as the values of the parameter $1/l^2$ increase (cf figure 1). Our results indicate that the shadow size of a regular AdS spacetime is larger compared to that of the Kerr black holes [83]. Table 1 provides detailed numerical values for shadow radius and distortion parameters across various spin parameter and free parameter values. The angular diameter of the black hole can be estimated via

$$\theta_{\rm d} = \frac{2}{r_o}\sqrt{\frac{A}{\pi}}, \tag{57}$$

where $r_o = 50M$ and A shadow area, and can be estimated via the shadow radius. Figure 7, illustrates how the area of the shadow image varies with the parameters $1/l^2$ and k. The area of the black hole shadow increases for the increasing values

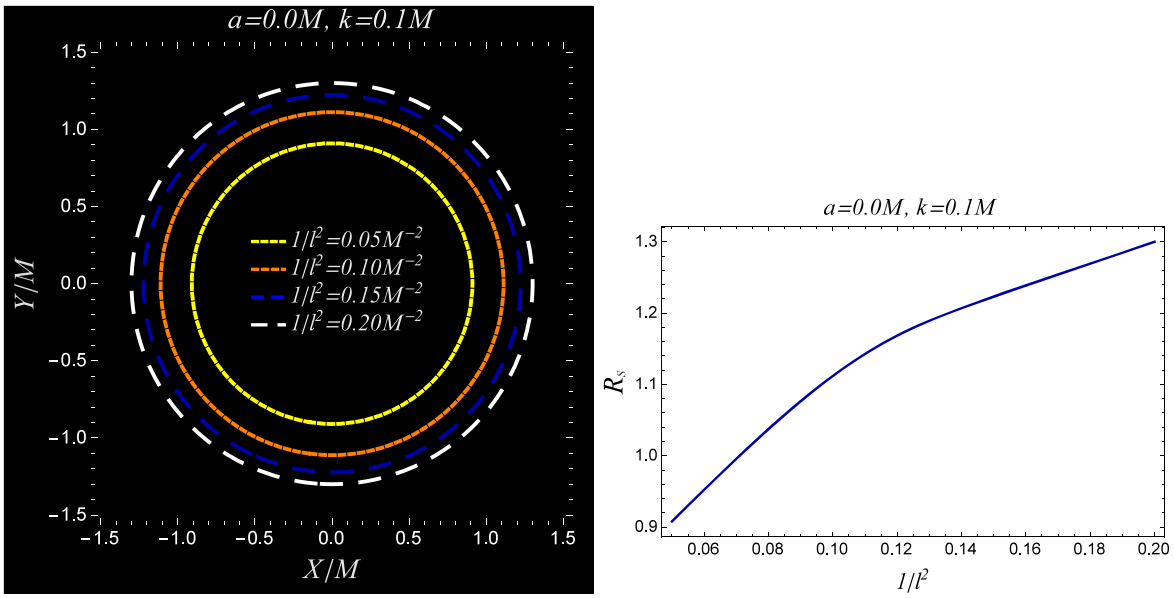

Figure 3. Non-spinning regular AdS black hole shadow with observable R_s for different values of k with $1/l^2$ at $r_O = 50$.

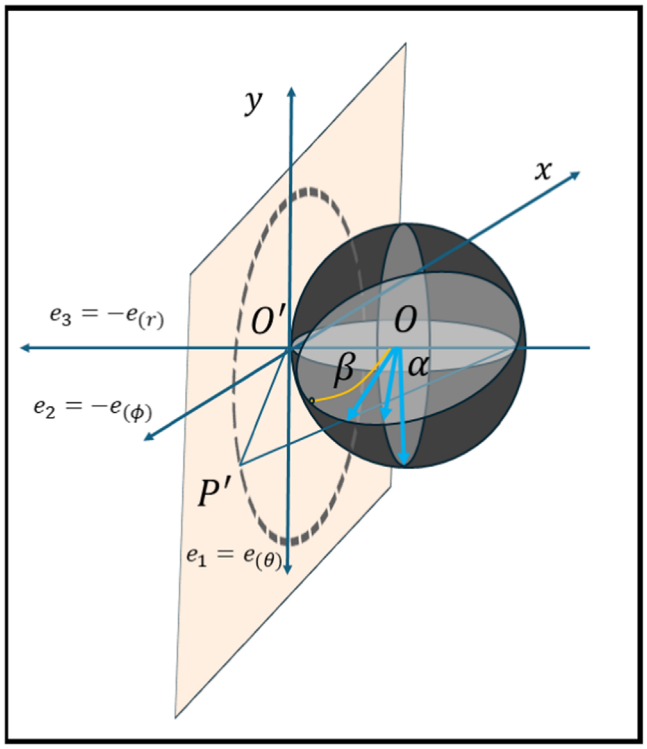

Figure 4. The celestial coordinates α and β are introduced to trace the paths of photon rays in the observer's frame. Using stereographic projection, we define a map from the celestial sphere to the observer [86].

of $1/l^2$ while it decreases with the parameter k. The variation in the angular diameter of the black hole shadow is illustrated in figure 8 for a static observer within the domain of outer communication. The angular diameter of regular AdS black hole shadow increases with $1/l^2$ and varies in the range of $2 \pm 0.52^\circ$ for $0.05 \leqslant 1/l^2 \leqslant 0.2$ with $0.05 \leqslant k \leqslant 0.2$.

5. Energy emission rate

As a good approximation, we can use the limiting constant value of the absorption cross-section for a nearly spherically symmetric black hole as

$$\sigma_{\rm lim} \approx \pi R_s^2. \tag{58}$$

We can use such limiting value of the geometric cross-section in order to calculate the energy emission rate

$$\frac{{\rm d}^2 E(\omega)}{{\rm d}\omega {\rm d}t} = \frac{2\pi^2 R_s^2}{{\rm e}^{\omega/T} - 1}\omega^3, \tag{59}$$

where ω is the frequency of the emitted photon and the temperature T of the nonsingular-AdS black hole in terms of the event horizon radius is expressed as

$$T = T_{\rm Kerr-AdS} - \frac{k(1 - R_+^2/l^2)}{4\pi R_+^2(R_+^2 + a^2)}, \tag{60}$$

where $T_{\rm Kerr\text{-}AdS}$ is the corresponding temperature for the Kerr-AdS black holes

$$T_{\rm Kerr-AdS} = \frac{R_+^2(1 + 3R_+^2/l^2) - a^2(1 - R_+^2/l^2)}{4\pi R_+(R_+^2 + a^2)}. \tag{61}$$

In figure 9 we have plotted the energy emission rate of the black hole with ω for different values of curvature radius term. It is shown in the figure that there exists a peak of energy emission rate, which decreases as we increase $1/l^2$ term and other black hole parameters.

6. Conclusion

In rotating Kerr spacetimes the shapes of black hole shadows get distorted mainly by the spin parameter a. In other theories of gravity *viz*. the MGs, some other parameters may enhance

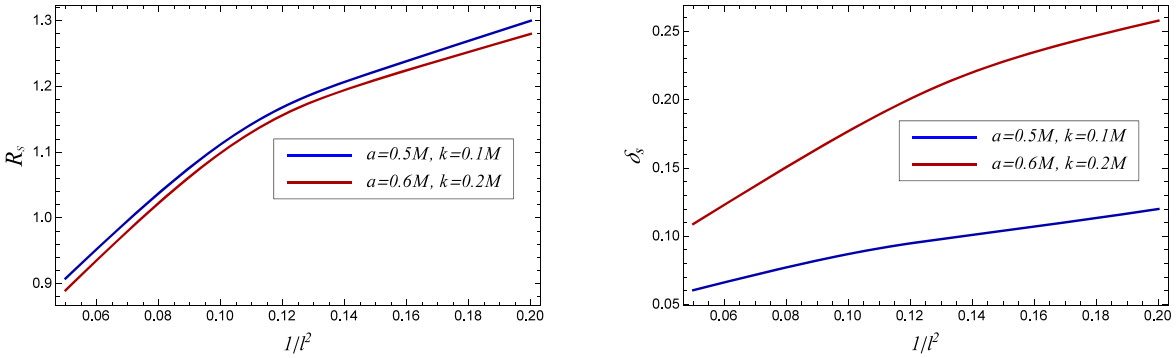

Figure 5. Plots showing the variation of observables R_s and δ_s with $1/l^2$ for different values of a and k at $r_O = 50$.

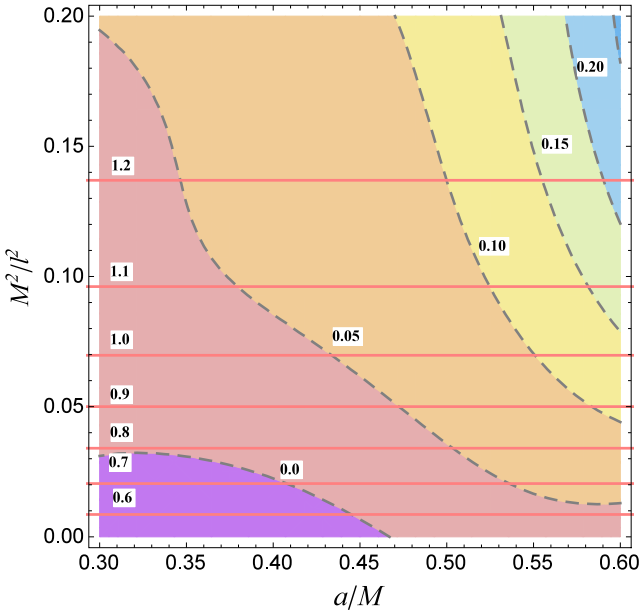

Figure 6. The contours of R_s (solid red lines) and δ_s (dashed gray lines) in $(a, 1/l^2)$ plane. The point of intersection of R_s and δ_s lines gives the values of black hole parameters.

Table 1. Variation of shadow radius and distortion parameter with parameter M^2/l^2.

$a = 0.5M$, $k = 0.1M$		
Radius of curvature (M^2/l^2)	Shadow radius (R_s/M)	Distortion parameter (δ_s)
0.05	0.90	0.06
0.10	1.11	0.08
0.15	1.22	0.10
0.20	1.30	0.12
$a = 0.6M$, $k = 0.2M$		
Radius of curvature M^2/l^2	Shadow radius (R_s/M)	Distortion parameter (δ_s)
0.05	0.89	0.11
0.10	1.09	0.17
0.15	1.21	0.23
0.20	1.28	0.27

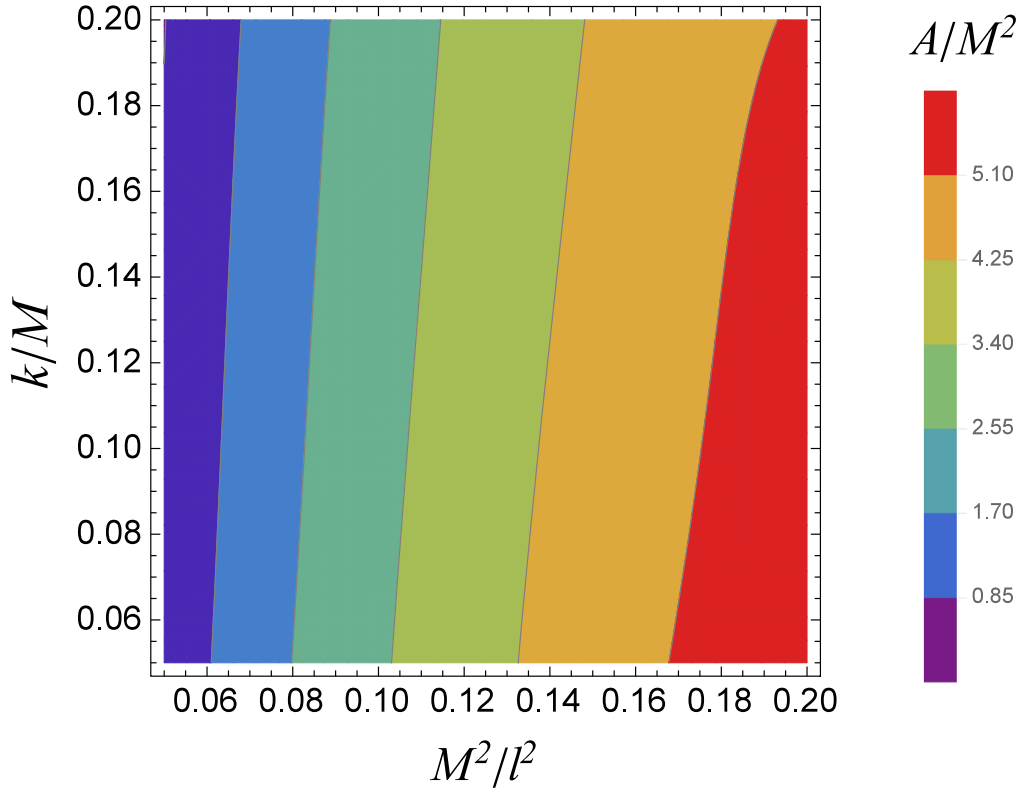

Figure 7. Variation of the Area of the black hole shadow with the black hole parameters.

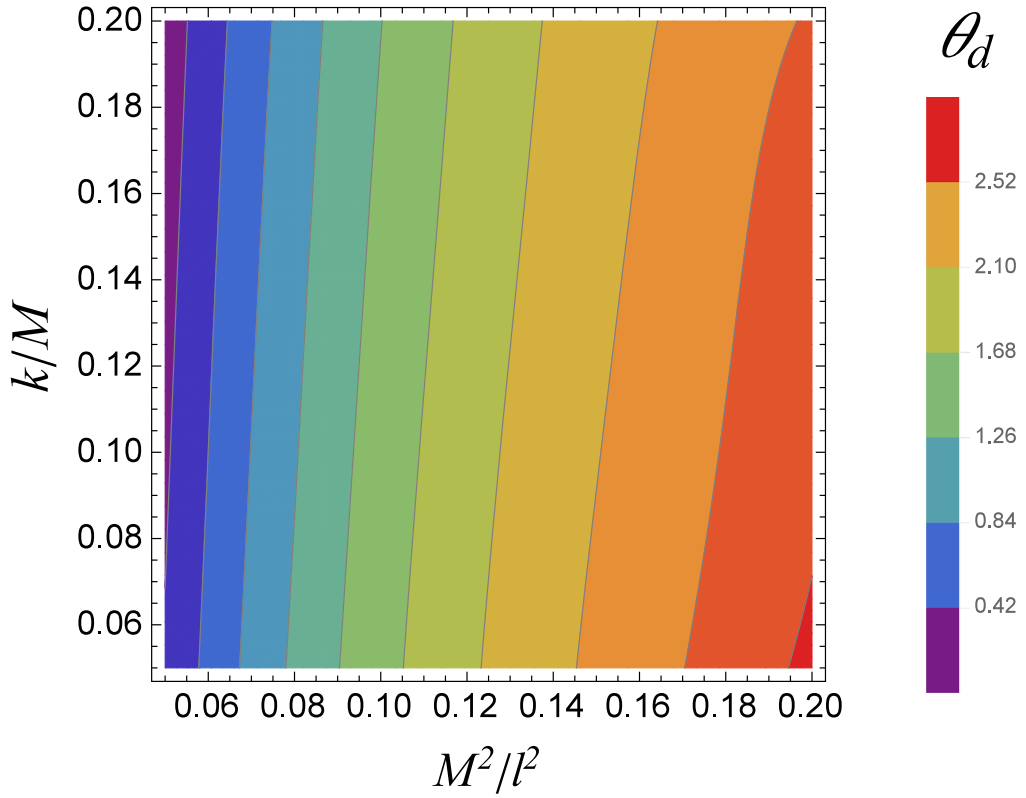

Figure 8. Variation of the angular diameter of the black hole shadow with the black hole parameters.

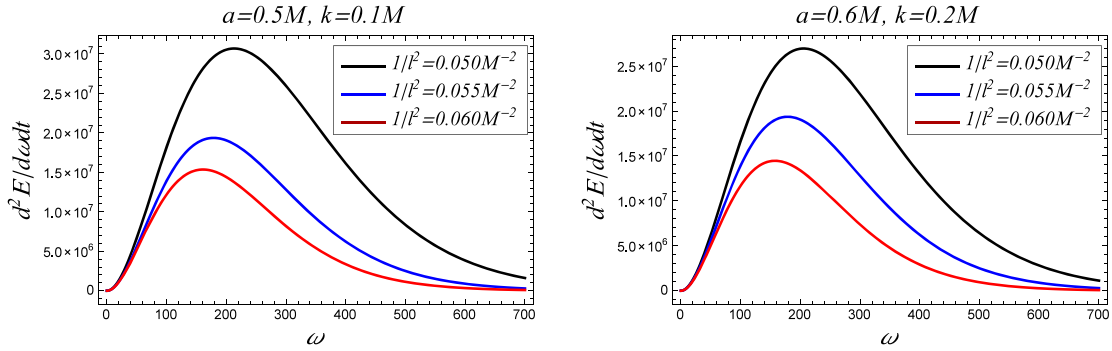

Figure 9. Plot showing the energy emission rate of the photon region.

or decrease the shadow of the black hole. In this paper, we have investigated the shadow of the rotating regular black hole in the presence of a cosmological constant. The size of the black hole shadow and distortion parameter increases with the increasing values of curvature radius parameter $1/l^2$. The black hole shadow appears smaller and more distorted in comparison to the regular and Kerr spacetime (cf figure 2). For a better understanding of black hole shadow, we have also calculated observables of the shadow radius R_s and the distortion parameter δ_s. The observables R_s and δ_s increase with the increasing values of $1/l^2$ and the effective size of the shadow radius decreases with the free parameter k. We also calculated the angular diameter of the black hole $\theta_d = 2 \pm 0.52^\circ$ for $0.05 \leqslant 1/l^2 \leqslant 0.2$ with $0.05 \leqslant k \leqslant 0.2$. From the study of energy emission rate, we conclude that the electromagnetic spectrum emitted by the shadow region of regular black holes in AdS spacetime decreases for the increasing values of the parameter $1/l^2$.

Acknowledgments

The research of MSA is supported by the National Post-doctoral Fellowship of the Science and Engineering Research Board (SERB), Department of Science and Technology (DST), Government of India, File No. PDF/2021/003491.

Credit authorship contribution statement

BPS: Methodology, software, visualization, investigation, writing - original draft. MSA: Software, formal analysis, writing - original draft. SGG: Conceptualization, supervision, investigation, writing - review and editing.

Declaration of competing interest

The author declares that they have no known competing financial interests or personal relationships that could have appeared to influence the work reported in this paper.

References

[1] Akiyama K(Event Horizon Telescope Collaboration) *et al* 2022 First sagittarius A* event horizon telescope results. I. The shadow of the supermassive black hole in the center of the milky way *Astrophys. J. Lett.* **930** L12
[2] Akiyama K(Event Horizon Telescope Collaboration) *et al* 2022 First sagittarius A* event horizon telescope results. II. EHT and multiwavelength observations, data processing, and calibration *Astrophys. J. Lett.* **930** L13
[3] Akiyama K(Event Horizon Telescope Collaboration) *et al* 2022 First sagittarius A* event horizon telescope results. III. imaging of the galactic center supermassive black hole *Astrophys. J. Lett.* **930** L14
[4] Akiyama K(Event Horizon Telescope Collaboration) *et al* 2022 First sagittarius A* event horizon telescope results. IV. variability, morphology, and black hole mass *Astrophys. J. Lett.* **930** L15
[5] Akiyama K(Event Horizon Telescope Collaboration) *et al* 2022 First sagittarius A* event horizon telescope results. V. Testing astrophysical models of the galactic center black hole *Astrophys. J. Lett.* **930** L16
[6] Akiyama K(Event Horizon Telescope Collaboration) *et al* 2022 First sagittarius A* event horizon telescope results. VI. Testing the black hole metric *Astrophys. J. Lett.* **930** L17
[7] Akiyama K(Event Horizon Telescope Collaboration) *et al* 2019 First M87 event horizon telescope results. I. The shadow of the supermassive black hole *Astrophys. J. Lett.* **875** L1
[8] Akiyama K(Event Horizon Telescope Collaboration) *et al* 2019 First M87 event horizon telescope results. II. Array and instrumentation *Astrophys. J. Lett.* **875** L2
[9] Akiyama K(Event Horizon Telescope Collaboration) *et al* 2019 First M87 event horizon telescope results. III. Data processing and calibration *Astrophys. J. Lett.* **875** L3
[10] Akiyama K(Event Horizon Telescope Collaboration) *et al* 2019 First M87 event horizon telescope results. IV. Imaging the central supermassive black hole *Astrophys. J. Lett.* **875** L4
[11] Akiyama K(Event Horizon Telescope Collaboration) *et al* 2019 First M87 event horizon telescope results. V. Physical origin of the asymmetric ring *Astrophys. J. Lett.* **875** L5
[12] Akiyama K(Event Horizon Telescope Collaboration) *et al* 2019 First M87 event horizon telescope results. VI. The shadow and mass of the central black hole *Astrophys. J. Lett.* **875** L6
[13] Bardeen J M 1973 *Black Holes* ed C De Witt and B S De Witt (Gorden and Breach) 215
[14] Young P J 1976 Capture of particles from plunge orbits by a black hole *Phys. Rev.* D **14** 3281
[15] Johannsen T 2013 Photon Rings around Kerr and Kerr-like Black Holes *Astrophys. J. Lett.* **777** 170

[16] de Vries A 1999 The apparent shape of a rotating charged black hole, closed photon orbits and the bifurcation set A_4 *Class. Quantum Grav.* **17** 123

[17] Amarilla L, Eiroa E F and Giribet G 2010 Null geodesics and shadow of a rotating black hole in extended Chern–Simons modified gravity *Phys. Rev.* D **81** 124045

[18] Amarilla L and Eiroa E F 2013 Shadow of a Kaluza–Klein rotating dilaton black hole *Phys. Rev.* D **87** 044057

[19] Yumoto A, Nitta D, Chiba T and Sugiyama N 2012 Shadows of multi-black holes: analytic exploration *Phys. Rev.* D **86** 103001

[20] Abdujabbarov A, Amir M, Ahmedov B and Ghosh S G 2016 Shadow of rotating regular black holes *Phys. Rev.* D **93** 104004

[21] Amir M and Ghosh S G 2016 Shapes of rotating nonsingular black hole shadows *Phys. Rev.* D **94** 024054

[22] Tsukamoto N, Li Z and Bambi C 2014 Constraining the spin and the deformation parameters from the black hole shadow *J. Cosmol. Astropart. Phys.* **1406** 043

[23] Hioki K and Maeda K I 2009 Measurement of the kerr spin parameter by observation of a compact object's shadow *Phys. Rev.* D **80** 024042

[24] Bambi C and Yoshida N 2010 Shape and position of the shadow in the $\delta = 2$ Tomimatsu–Sato space-time *Class. Quant. Grav.* **27** 205006

[25] Goddi C *et al* 2016 BlackHoleCam: fundamental physics of the Galactic center *Int. J. Mod. Phys.* D **26** 1730001

[26] Takahashi R 2005 Black hole shadows of charged spinning black holes *Publ. Astron. Soc. Jap.* **57** 273

[27] Wei S W and Liu Y X 2013 Observing the shadow of Einstein–Maxwell-Dilaton-Axion black hole *J. Cosmol. Astropart. Phys.* **11** 063

[28] Abdujabbarov A, Atamurotov F, Kucukakca Y, Ahmedov B and Camci U 2013 Shadow of Kerr-Taub-NUT black hole *Astrophys. Space Sci.* **344** 429

[29] Amarilla L and Eiroa E F 2012 Shadow of a rotating braneworld black hole *Phys. Rev.* D **85** 064019

[30] Bambi C and Freese K 2009 Apparent shape of super-spinning black holes *Phys. Rev.* D **79** 043002

[31] Atamurotov F, Abdujabbarov A and Ahmedov B 2013 Shadow of rotating non-Kerr black hole *Phys. Rev.* D **88** 064004

[32] Wang M, Chen S and Jing J 2017 Shadow casted by a Konoplya–Zhidenko rotating non-Kerr black hole *J. Cosmol. Astropart. Phys.* **1710** 051

[33] Schee J and Stuchlik Z 2009 Optical phenomena in the field of braneworld Kerr black holes *Int. J. Mod. Phys.* D **18** 983

[34] Grenzebach A, Perlick V and Lämmerzahl C 2014 Photon Regions and Shadows of Kerr–Newman-NUT Black Holes with a Cosmological Constant *Phys. Rev.* D **89** 124004

[35] Singh B P 2022 Rotating charged black hole shadow in quintessence *Ann. Phys.* **441** 168892

[36] Kumar R, Singh B P and Ghosh S G 2020 Shadow and deflection angle of rotating black hole in asymptotically safe gravity *Ann. Phys.* **420** 168252

[37] Kumar R, Singh B P, Ali M S and Ghosh S G 2021 Shadows of black hole surrounded by anisotropic fluid in Rastall theory *Phys. Dark Univ.* **34** 100881

[38] Kumar R and Ghosh S G 2020 Rotating black holes in 4D Einstein–Gauss–Bonnet gravity and its shadow *J. Cosmol. Astropart. Phys.* **07** 053

[39] Narzilloev B, Hussain I, Abdujabbarov A and Ahmedov B 2022 Optical properties of an axially symmetric black hole in the Rastall gravity *Eur. Phys. J. Plus* **137** 645

[40] Wei S W, Zou Y C, Liu Y X and Mann R B 2019 Curvature radius and Kerr black hole shadow *J. Cosmol. Astropart. Phys.* 030

[41] Papnoi U and Atamurotov F 2022 Rotating charged black hole in 4D Einstein–Gauss–Bonnet gravity: Photon motion and its shadow *Phys. Dark Univ.* **35** 100916

[42] Atamurotov F, Papnoi U and Jusufi K 2022 Shadow and deflection angle of charged rotating black hole surrounded by perfect fluid dark matter *Class. Quantum Grav.* **39** 025014

[43] Ovalle J, Contreras E and Stuchlik Z 2021 Kerr–de Sitter black hole revisited *Phys. Rev.* D **103** 084016

[44] Ovalle J 2022 Warped vacuum energy by black holes *Eur. Phys. J.* C **82** 170

[45] Guo S, Li G R and Liang E W 2022 Influence of accretion flow and magnetic charge on the observed shadows and rings of the Hayward black hole *Phys. Rev.* D **105** 023024

[46] Guo S, Li G R and Liang E W 2022 Observable characteristics of the charged black hole surrounded by thin disk accretion in Rastall gravity *Class. Quantum Grav.* **39** 135004

[47] Guo S, He K J, Li G R and Li G P 2021 The shadow and photon sphere of the charged black hole in Rastall gravity *Class. Quantum Grav.* **38** 165013

[48] Guo S, Li G R and Li G P 2022 Shadow thermodynamics of an AdS black hole in regular spacetime *Chin. Phys.* C **46** 095101

[49] Uniyal A, Pantig R C and Övgün A 2023 Probing a non-linear electrodynamics black hole with thin accretion disk, shadow, and deflection angle with M87* and Sgr A* from EHT *Phys. Dark Univ.* **40** 101178

[50] Li P C, Guo M and Chen B 2020 Shadow of a spinning black hole in an expanding universe *Phys. Rev.* D **101** 084041

[51] Zhang Z, Yan H, Guo M and Chen B 2023 Shadows of Kerr black holes with a Gaussian-distributed plasma in the polar direction *Phys. Rev.* D **107** 024027

[52] Hou Y, Guo M and Chen B 2021 Revisiting the shadow of braneworld black holes *Phys. Rev.* D **104** 024001

[53] Perlick V, Tsupko O Y and Bisnovatyi-Kogan G S 2015 Influence of a plasma on the shadow of a spherically symmetric black hole *Phys. Rev.* D **92** 104031

[54] Atamurotov F and Ahmedov B 2015 Optical properties of black hole in the presence of plasma: shadow *Phys. Rev.* D **92** 084005

[55] Abdujabbarov A, Toshmatov B, Stuchlik Z and Ahmedov B 2016 Shadow of the rotating black hole with quintessential energy in the presence of plasma *Int. J. Mod. Phys.* D **26** 1750051

[56] Papnoi U, Atamurotov F, Ghosh S G and Ahmedov B 2014 Shadow of five-dimensional rotating Myers–Perry black hole *Phys. Rev.* D **90** 024073

[57] Singh B P and Ghosh S G 2018 Shadow of Schwarzschild–Tangherlini black holes *Annals Phys.* **395** 127

[58] Amir M, Singh B P and Ghosh S G 2018 Shadows of rotating five-dimensional charged EMCS black holes *Eur. Phys. J.* C **78** 399

[59] Abdujabbarov A, Atamurotov F, Dadhich N, Ahmedov B and Stuchlik Z 2015 Energetics and optical properties of 6-dimensional rotating black hole in pure Gauss–Bonnet gravity *Eur. Phys. J.* C **75** 399

[60] Atamurotov F, Jusufi K, Jamil M, Abdujabbarov A and Azreg-Aïnou M 2021 Axion-plasmon or magnetized plasma effect on an observable shadow and gravitational lensing of a Schwarzschild black hole *Phys. Rev.* D **104** 064053

[61] Cunha P V P, Herdeiro C A R, Radu E and Runarsson H F 2015 Shadows of Kerr black holes with scalar hair *Phys. Rev. Lett.* **115** 211102

[62] Cunha P V P, Herdeiro C A R, Radu E and Runarsson H F 2016 Shadows of Kerr black holes with and without scalar hair *Int. J. Mod. Phys.* D **25** 1641021

[63] Eiroa E F and Sendra C M 2018 Shadow cast by rotating braneworld black holes with a cosmological constant *Eur. Phys. J.* C **78** 91

[64] Belhaj A, Belmahi H and Benal M 2021 Superentropic AdS black hole shadows *Phys. Lett.* B **821** 136619

[65] Belhaj A, Belmahi H, Benali M, El Moumni H, Essebani M A and Sedra M B 2022 Optical shadows of rotating Bardeen-AdS black holes *Mod. Phys. Lett.* A **37** 2250032
[66] Belhaj A, Benali M, Balali A E, Hadri W E and Moumni H E 2021 Cosmological constant effect on charged and rotating black hole shadows *Int. J. Geom. Meth. Mod. Phys.* **18** 2150188
[67] Afrin M and Ghosh S G 2022 Estimating the Cosmological Constant from Shadows of Kerr–de Sitter Black Holes *Universe* **8** 52
[68] Ali M S, Ghosh S G and Maharaj S D 2020 Effective thermodynamics and critical phenomena of rotating regular-de Sitter black holes *Class. Quantum Grav.* **37** 185003
[69] Kumar A, Ghosh S G and Maharaj S D 2020 Nonsingular black hole chemistry *Phys. Dark Univ.* **30** 100634
[70] Ayon-Beato E and Garcia A 2000 The Bardeen model as a nonlinear magnetic monopole *Phys. Lett.* B **493** 149
[71] Ghosh S G, Singh D V and Maharaj S D 2018 Regular black holes in Einstein–Gauss–Bonnet gravity *Phys. Rev.* D **97** 104050
[72] Nam C H 2018 Non-linear charged AdS black hole in massive gravity *Eur. Phys. J.* C **78** 1016
[73] Toshmatov B, Stuchlìk Z and Ahmedov B 2017 Generic rotating regular black holes in general relativity coupled to nonlinear electrodynamics *Phys. Rev.* D **95** 084037
[74] Erbin H 2017 Janis–Newman algorithm: generating rotating and NUT charged black holes *Universe* **3** 19
[75] Ghosh S G 2015 A nonsingular rotating black hole *Eur. Phys. J.* C **75** 532
[76] Plebanski J F and Demianski M 1976 Rotating, charged, and uniformly accelerating mass in general relativity *Ann. Phys.* **98**
[77] Xu Z and Wang J 2017 Kerr–Newman-AdS black hole in quintessential dark energy *Phys. Rev.* D **95** 064015
[78] Bambi C 2013 Measuring the Kerr spin parameter of a non-Kerr compact object with the continuum-fitting and the iron line methods *J. Cosmol. Astropart. Phys.* **1308** 055
[79] Bambi C 2013 Testing the space-time geometry around black hole candidates with the available radio and X-ray data *Astron. Rev.* **8** 4
[80] Bambi C 2011 Testing the Kerr black hole hypothesis *Mod. Phys. Lett.* A **26** 2453
[81] Cardenas-Avendano A, Jiang J and Bambi C 2016 Testing the Kerr black hole hypothesis: comparison between the gravitational wave and the iron line approaches *Phys. Lett.* B **760** 254
[82] Carter B 1968 Global structure of the Kerr family of gravitational fields *Phys. Rev.* **174** 1559
[83] Chandrasekhar S 1992 *The Mathematical Theory of Black Holes* (Oxford: Oxford University Press)
[84] Wang X, Hou Y and Guo M 2023 How different are shadows of compact objects with and without horizons? *J. Cosmol. Astropart. Phys.* 036
[85] Wang X, Wang X, Zhang H Q and Guo M 2024 Is a photon ring invariably a closed structure? arXiv:2405.05011
[86] Hu Z, Zhong Z, Li P C, Guo M and Chen B 2021 QED effect on a black hole shadow *Phys. Rev.* D **103** 044057